J. Fluid Mech. (1988), *vol.* 196, *pp.* 495–511
Printed in Great Britain

Instabilities caused by oscillating accelerations normal to a viscous fluid–fluid interface

By DAVID JACQMIN AND WALTER M. B. DUVAL
NASA Lewis Research Center, Cleveland, OH 44135, USA

(Received 9 September 1987 and in revised form 19 April 1988)

Two incompressible viscous fluids with different densities meet at a planar interface. The fluids are subject to an externally imposed oscillating acceleration directed normal to the interface. The resulting basic-state flow is motionless with an internal pressure oscillation. We discuss the linear evolution of perturbations to this basic state. General viscosities and densities for the two fluids are considered but a Boussinesq equal-viscosity approximation is discussed in particular detail. For this case we show that the linear evolution of a perturbation to the interface subject to an arbitrary oscillating acceleration is governed by a single integro–differential equation. We apply a Floquet analysis to the fluid system for the case of sinusoidal forcing. Parameter regions of subharmonic, harmonic, and untuned modes are delineated. The critical Stokes–Reynolds number is found as a function of the surface tension and the difference in density and viscosity between the two fluids. The most unstable perturbation wavelengths are determined. For zero surface tension these are found to be short, on the order of a small multiple of the Stokes viscous lengthscale. The critical Stokes–Reynolds number and the most unstable perturbation wavelengths are found to be insensitive to the degree of density and viscosity differences between the two fluids.

1. Introduction

The mixing of two viscous fluids by shaking is a common occurrence. This paper discusses a model problem as a step towards understanding the initiation of mixing caused by low-amplitude oscillations. We investigate the stability of a planar, viscous fluid–fluid interface subject to oscillating normal accelerations.

The treatment of the problem herein idealizes the fluid system as being in an infinite domain. The linear evolution of a perturbation to this interface then depends on four non-dimensional parameters: the Stokes–Reynolds number, the surface-tension parameter, a parameter for the density difference between the two fluids, and a parameter for the absolute viscosity difference. To simplify the analysis and results the latter two parameters are neglected in much of this paper. Section 4 presents numerical evidence that this neglect is usually acceptable. Also, we primarily consider the case of zero surface tension. This is because we have a particular interest in the very short-wavelength instabilities generated in the zero-surface-tension case. These are so small as to be difficult to resolve in Navier–Stokes numerical calculations, yet they may have a significant effect on transport through an interface and in determining larger scale interface evolution. An additional reason for restricting consideration of the non-zero-surface-tension case is that even weak surface tension can often overwhelm the effects of viscosity, making the complexity of a viscous analysis superfluous. Surface tension is considered here primarily

to demonstrate how the fluid system's behaviour changes radically with its introduction.

This work was initially motivated by a desire to understand the potential effects of oscillating accelerations on space-based materials processing experiments. A particular example of such an experiment is crystal growth using counterdiffusion. It may be possible for g-jitter (random accelerations) to drive wave formation in the sharp interior concentration and density-gradient layers that can occur with this technique. Such wave formation could lead to an increase in crystal growth defects (Galster & Nielsen 1984). The problem discussed here, accelerations normal to an interface, is one of two model problems relevant to the effects of g-jitter on sharp fluid-density gradients. The other problem is g-jitter parallel to the interface. This forces a viscous, oscillating Kelvin–Helmholtz flow. This problem is undoubtedly the more significant of the two, but it is also considerably more difficult. It is hoped that the results presented in this paper will lay some groundwork for the analysis of the parallel case.

The model problem discussed in this paper can be considered an extension and generalization of the linear stability problem posed by Faraday resonances (Faraday 1831). In the classic formulation of this problem, one considers an inviscid fluid with a free surface subject to a stabilizing mean gravity and accelerations normal to the surface. This was first successfully investigated analytically by Benjamin & Ursell (1954). For the case of sinusoidal accelerations, they showed that the evolution of each mode of oscillation of the fluid is determined by Mathieu's equation:

$$\frac{\mathrm{d}^2\psi}{\mathrm{d}t^2} + (\delta + \epsilon \cos t)\,\psi = 0, \tag{1}$$

where ψ is the amplitude of the mode and δ and ϵ are mode-dependent constants. The stability bounds of the Mathieu equation (Mclachlan 1947) correspond to the onset of wave motion in the fluid. Finite-amplitude behaviour of this system has since been investigated by Dodge, Kana & Abramson (1965), Ockendon & Ockendon (1973), Henstock & Sani (1974), and Miles (1984). None of these papers considers viscous terms, but some work that considers viscous effects for a similar system has been recently carried out by Hasegawa (1983) and Hasegawa, Umahara & Atsumi (1984). Using highly truncated spectral approximations, they considered the stability of oscillated thin viscous fluid layers.

The literature on flows caused or affected by g-jitter goes back to the early sixties. Gebhart (1963), Spradley, Bougeois & Lin (1975), and Kamotani, Prasad & Ostrach (1981) discuss the effect of g-jitter on heat transfer and on temperature oscillations in fluids. Gebhart concluded that g-jitter generally enhances heat and mass transport while Kamotani *et al.* found that temperature oscillations induced by g-jitter might be significant in influencing the dynamics of crystal growth. Related to these papers are several papers on the interaction of mechanical vibrations and convective instabilities, by, among others, Donnelly, Reif & Suhl (1962), Gresho & Sani (1970), and Burde (1970). Most of the research to date has considered g-jitter-influenced flows with only smooth distributions of temperature and/or composition. One exception is Spradley *et al.*, which briefly discusses free-surface effects noticed in some numerical calculations.

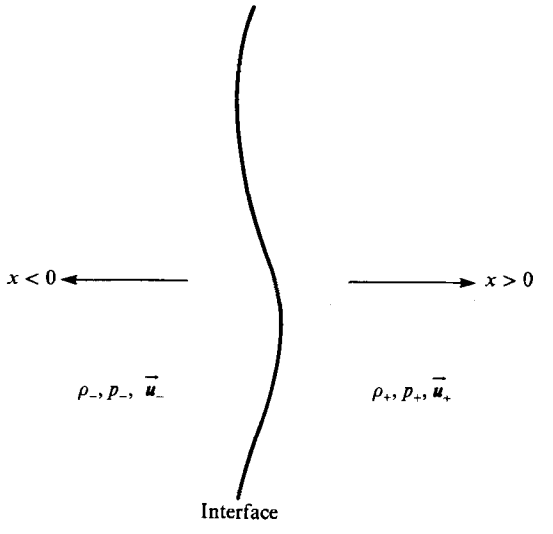

FIGURE 1. The fluid system.

2. Formulation

The fluid system is shown in figure 1. Two incompressible fluids with differing densities and viscosities meet at an interface centred on $x = 0$. The denser fluid is to the right of the interface. Molecular diffusivity, which for most fluids is very small compared to viscosity, is neglected. With this idealization, even with no surface tension, an initially sharp fluid–fluid interface remains sharp as it evolves. The momentum equations for the fluids are

$$\rho_\pm \frac{\mathrm{D}\boldsymbol{u}_\pm}{\mathrm{D}t} - \mu_\pm \nabla^2 \boldsymbol{u}_\pm = -\nabla p_\pm + \boldsymbol{i} A g(\omega t) \rho_\pm, \tag{2}$$

where the plus and minus subscripts refer, respectively, to the right and left fluids. $Ag(\omega t)$ is the imposed oscillating acceleration, with $g(t)$ having mean-square amplitude $1/\sqrt{2}$, and a dominant frequency of $1/2\pi$. Since we are interested in g-jitter we limit $g(t)$ to having zero mean. The inclusion of a non-zero mean $g(t)$ would be quite straightforward.

The equations can be non-dimensionalized and somewhat simplified as follows. First, we set $\rho_+ - \rho_- = \Delta\rho$, $\mu_+ - \mu_- = \Delta\mu$, $\frac{1}{2}(\rho_- + \rho_+) = \rho_\mathrm{a}$, $\frac{1}{2}(\mu_- + \mu_+) = \mu_\mathrm{a}$, and $\mu_\mathrm{a}/\rho_\mathrm{a} = \nu_\mathrm{a}$. Subtracting out $Ag(\omega t)\rho_\mathrm{a} x$ from both p_- and p_+ and then scaling (2) with the Stokes lengthscale $(2\nu_\mathrm{a}/\omega)^{\frac{1}{2}}$ the timescale $1/\omega$, the velocity scale $\mathrm{A}(\Delta\rho/\rho_\mathrm{a})(1/\omega)$, and the pressure scale $A\Delta\rho(\nu_\mathrm{a}/2\omega)^{\frac{1}{2}}$, the non-dimensionalized momentum equations for the bulk fluids become

$$2(1 \pm \Theta_\rho)\frac{\partial \boldsymbol{u}_\pm}{\partial t} + (1 \pm \Theta_\rho) R_\mathrm{S}(\boldsymbol{u}_\pm \cdot \nabla \boldsymbol{u}_\pm) - (1 \pm \Theta_\mu)\nabla^2 \boldsymbol{u}_\pm = -\nabla p_\pm \pm \boldsymbol{i} g(t). \tag{3}$$

Here R_S is the Stokes–Reynolds number,

$$R_\mathrm{S} = A\frac{\Delta\rho}{\rho_\mathrm{a}}\left(\frac{2}{\nu_\mathrm{a}\omega^3}\right)^{\frac{1}{2}}.$$

$\Theta_\rho = \Delta\rho/2\rho_\mathrm{a}$ and $\Theta_\mu = \Delta\mu/2\mu_\mathrm{a}$. Θ_ρ can vary from 0 to 1 and Θ_μ can vary from -1 to 1.

We are interested in the evolution of the interface from some initial perturbation. This can be treated as a linear stability problem in which the basic state is motionless with an internal pressure oscillation caused by the imposed acceleration. With the basic-state interface at $x = 0$, the basic-state pressure is $g(t)|x|$. Linearized perturbations to this state obey

$$2(1 \pm \Theta_\rho)\frac{\partial \boldsymbol{u}_\pm}{\partial t} - (1 \pm \Theta_\mu)\nabla^2 \boldsymbol{u}_\pm = -\nabla p_\pm, \quad \nabla \cdot \boldsymbol{u}_\pm = 0. \tag{4a, b}$$

Interfacial boundary conditions at $x = 0$ are that the velocities and stresses be continuous. The stress conditions can be expressed in terms of the velocities, pressures and the interface position h as

$$\tau_{xy}: (1+\Theta_\mu)\left(\frac{\partial u_+}{\partial y} + \frac{\partial v_+}{\partial x}\right) = (1-\Theta_\mu)\left(\frac{\partial u_-}{\partial y} + \frac{\partial v_-}{\partial x}\right), \tag{5a}$$

$$\tau_{xz}: (1+\Theta_\mu)\left(\frac{\partial u_+}{\partial z} + \frac{\partial w_+}{\partial x}\right) = (1-\Theta_\mu)\left(\frac{\partial u_-}{\partial z} + \frac{\partial w_-}{\partial x}\right), \tag{5b}$$

$$\tau_{xx}: p_+ - p_- = 4\Theta_\mu \frac{\partial u}{\partial x} - 2g(t)\,h + 2T\left(\frac{\partial^2 h}{\partial y^2} + \frac{\partial^2 h}{\partial z^2}\right). \tag{5c}$$

T is the non-dimensional surface-tension parameter

$$T = \frac{1}{2}\frac{\omega}{\nu_a}\frac{1}{\Delta\rho}\frac{\tilde{T}}{A},$$

where $\tilde{T}$ is the original dimensional coefficient.

By application of the continuity equation, (4)–(5) can be rewritten in terms of just u, p and h. Next, the equations allow the Fourier decomposition $(u, p, h) \Rightarrow \cos \alpha z \cos \beta y (u^*, p^*, h^*)$. The resulting one-dimensional system of equations is

$$2(1 \pm \Theta_\rho)\frac{\partial u_\pm}{\partial t} - (1 \pm \Theta_\mu)\left(\frac{\partial^2 u_\pm}{\partial x^2} - \gamma^2 u_\pm\right) = -\frac{\partial p_\pm}{\partial x}, \tag{6a}$$

$$\frac{\partial^2 p_\pm}{\partial x^2} - \gamma^2 p_\pm = 0, \tag{6b}$$

where the asterisk superscript has been dropped and where $\gamma^2 = \alpha^2 + \beta^2$. The interfacial boundary conditions become

$$u_+ = u_-, \quad \frac{\partial u_+}{\partial x} = \frac{\partial u_-}{\partial x}, \quad p_+ - p_- = 4\Theta_\mu \frac{\partial u}{\partial x} - 2(g(t) + \gamma^2 T)\,h, \tag{7a, b, c}$$

$$\frac{\partial p_+}{\partial x} - \frac{\partial p_-}{\partial x} = -4\gamma^2 \Theta_\mu u - 4\Theta_\rho \frac{\partial u}{\partial t}. \tag{7d}$$

The kinematic equation for h is

$$2\frac{\mathrm{d}h}{\mathrm{d}t} = R_s u. \tag{8}$$

The conditions at $\pm\infty$ are that u and p are evanescent.

3. The Boussinesq equal-viscosity case

Adoption of the Boussinesq approximation ($\Theta_\rho = 0$) and neglect of Θ_μ allows a considerable simplification of (6)–(8). (u, p)-eigensolutions are then necessarily of (even, odd) symmetry. Thus only the domain $x > 0$ must be considered. Accordingly, we drop the + and − subscripts. The solution for p in $x > 0$ is $-(g(t)+\gamma^2 T)\,h(t)\,\mathrm{e}^{-\gamma x}$ and the equations for u and h reduce to

$$2\frac{\partial u}{\partial t}-\left(\frac{\partial^2 u}{\partial x^2}-\gamma^2 u\right)=-\gamma(g(t)+\gamma^2 T)\,h\,\mathrm{e}^{-\gamma x},\quad 2\frac{\partial h}{\partial t}=R_{\mathrm{S}}\,u,\quad \left.\frac{\partial u}{\partial x}\right|_0=0. \quad (9a,b,c)$$

Formally, the Bousinesq approximation amounts to the limit $\Delta\rho\to 0$ while $A\Delta\rho$ remains constant. Informally, it has the usual meaning: we are neglecting variations in density except when it multiplies the imposed acceleration. The solutions to (6)–(7) vary smoothly as the Boussinesq limit is approached.

3.1. *Asymptotic results for general forcing*

If the viscous terms in $(9a)$ are neglected, then $(9a, b)$ can be easily combined to form an ordinary differential equation for h:

$$\frac{\mathrm{d}^2 h}{\mathrm{d}t^2}+(\tfrac{1}{4}\gamma^3 R_{\mathrm{S}} T+\tfrac{1}{4}\gamma R_{\mathrm{S}}\,g(t))\,h=0. \quad (10)$$

If, in addition, $g(t)=\cos t$, then (10) becomes Mathieu's equation, given as (1), with $\delta=\frac{1}{4}\gamma^3 R_{\mathrm{S}} T$ and $\epsilon=\frac{1}{4}\gamma R_{\mathrm{S}}$. Though its inclusion of R_{S} disguises it, (10) is basically the equation for the inviscid case. A redimensionalization of γ and T cancels out the ν_{a} in the denominator of R_{S}. Alternatively, the inviscid case can be viewed as represented by (10) with the limit of $R_{\mathrm{S}}\to\infty$ while γR_{S} and $\gamma^2 T$ remain finite. γ goes to zero not because the dimensional wavelength is becoming infinitely long but because the Stokes lengthscale goes to zero with the viscosity. The correct lengthscale for the inviscid case is A/ω^2.

With the inclusion of the viscous terms in $(9a)$, (10) becomes an integro–differential equation. To derive this, set

$$\frac{\partial u}{\partial t}=u_{,t}=u_{1,t}(t)\,\mathrm{e}^{-\gamma x}+u_{2,t}(t,x),\quad u_{1,t}=-\tfrac{1}{2}\gamma(g(t)+\gamma^2 T)\,h(t).$$

Then, from $(9a, c)$, $u_{2,t}$ obeys

$$2\frac{\partial u_{2,t}}{\partial t}=\frac{\partial^2 u_{2,t}}{\partial x^2}-\gamma^2 u_{2,t},\quad \left.\frac{\partial u_{2,t}}{\partial x}\right|_0=-\tfrac{1}{2}\gamma^2(g(t)+\gamma^2 T)\,h. \quad (11a,b)$$

The solution to (11) for initial conditions set at $t=0$ (see Carslaw & Jaeger 1959, pp. 53, 75–76) is

$$u_{2,t}(t,x=0)=\frac{2}{(2\pi t)^{\frac{1}{2}}}\,\mathrm{e}^{-\frac{1}{2}\gamma^2 t}\int_0^\infty u_{2,t}(t=0,x')\,\mathrm{e}^{-\frac{x'^2}{2t}}\,\mathrm{d}x'$$
$$+\frac{1}{(2\pi)^{\frac{1}{2}}}\tfrac{1}{2}\gamma^2\int_0^t(g(\tau)+\gamma^2 T)\,h(\tau)\frac{\mathrm{e}^{-\frac{1}{2}\gamma^2(t-\tau)}}{(t-\tau)^{\frac{1}{2}}}\,\mathrm{d}\tau. \quad (12)$$

Since we are interested in the long-time stability of the system, the first integral,

which fades exponentially to zero, can be neglected and the limits on the second can be changed from 0 to t to $-\infty$ to t. Since

$$2\frac{\mathrm{d}^2 h}{\mathrm{d}t^2} = R_S(u_{1,t}(t) + u_{2,t}(t, x = 0)),$$

we obtain

$$\frac{\mathrm{d}^2 h}{\mathrm{d}t^2} + \tfrac{1}{4}\gamma R_S(g(t) + \gamma^2 T)\, h = \frac{\gamma}{(2\pi)^{\frac{1}{2}}} \int_{-\infty}^{t} \tfrac{1}{4}\gamma R_S(g(\tau) + \gamma^2 T)\, h(\tau) \frac{\mathrm{e}^{-\frac{1}{2}\gamma^2(t-\tau)}}{(t-\tau)^{\frac{1}{2}}} \mathrm{d}\tau. \tag{13}$$

Neglect of the integral in (13) is often acceptable when γ is small enough but γ does not necessarily have to be $\ll 1$. For example, the rescaling $t = R_S^{-\frac{2}{3}} t', \gamma = R_S^{\frac{1}{3}} \gamma'$ factors out R_S and is useful for the case of large R_S and $T = 0$. Then $g(t')$ is slowly varying and a quasi-static analysis shows that the integral can be neglected, to a first approximation, when $\gamma^3 \ll R_S$. A similar approach can be used when $R_S T$ is large. Then the integral can be neglected, for many purposes, when $\gamma \ll R_S T$.

A good way to look at the effects of the integral in (13) is to consider the difference in solution behaviour between (10) and (13) as γ becomes large. As γ increases, solutions to (10) with $T = 0$ become more and more unstable; in fact, growth rates increase without bound as $\gamma \to \infty$. For $T \neq 0$ solutions to (10) become neutrally stable and rapidly oscillatory. In (13), the integral acts as a delayed approximate cancellation of the multiplier of h on the left-hand side of (13). This cancellation effect corresponds to the viscous diffusion of any evolved momentum away from the interface. As γ increases this cancellation is accomplished increasingly quickly and completely. The result is that h for large γ always becomes stable. With $T = 0$, h decays very slowly while with $T \neq 0$ its rate of decay increases linearly with γ.

In order to demonstrate the above we simplify (13) as follows. For large γ, the integrand in (13) can be expressed in terms of an asymptotic series in inverse powers of γ. Taking advantage of the fact that the integrand for large γ is significant only near $\tau = t$, the integrand quantity

$$f(\tau) = \tfrac{1}{4}\gamma R_S(g(\tau) + \gamma^2 T)\, h(\tau)$$

can be adequately represented, provided that $g(\tau)$ and $h(\tau)$ are sufficiently slowly varying, by a truncated Taylor series about t. Then the right-hand side of (13) can be integrated term by term to yield

$$\sum_{n=0}^{N} (-1)^n \left(\frac{1}{n!}\right)^2 \frac{(2n)!}{2^n \gamma^{2n}} f^{(n)}(t),$$

where N is the number of derivatives of the Taylor series retained in the truncation. If N is taken to be zero, then (13) becomes simply $\mathrm{d}^2 h/\mathrm{d}t^2 = 0$, demonstrating the cancellation effect of the integral. For general N, (13) becomes, after one integration,

$$\frac{\mathrm{d}h}{\mathrm{d}t} = \sum_{n=1}^{N} (-1)^n \left(\frac{1}{n!}\right)^2 \frac{(2n)!}{2^n \gamma^{2n}} f^{(n-1)}(t). \tag{14}$$

Note that the right-hand side of (14) is equal, to within the accuracy of the present approximation, to $\frac{1}{2}R_S u(t, x = 0)$. The constant of integration has been set equal to zero in (14) because a time-independent component of u is inconsistent with solutions for u of the homogenous part of (9a, c).

We now consider the truncation $N = 2$. For this case, after some manipulation,

$$\frac{\mathrm{d}h}{\mathrm{d}t} = \frac{-\frac{1}{4}\frac{R_S}{\gamma}(g(t)+\gamma^2 T)+\frac{3}{8}\frac{R_S}{\gamma^3}\frac{\mathrm{d}g}{\mathrm{d}t}}{1-\frac{3}{8}\frac{R_S}{\gamma^3}(g(t)+\gamma^2 T)}h = r(t)\,h. \tag{15}$$

Two significant conclusions can be drawn from (15). First, as γ becomes large h oscillates with the same dominant frequency as g; there is no subharmonic, higher harmonic, or untuned behaviour. Secondly, h is stable. The average rate of decay of h is equal to the average of $r(t)$. This average is also an approximation to the Floquet exponent for the approximated solution. The average of $r(t)$ is

$$\overline{r(t)} = -\frac{1}{2\pi}\int_0^{2\pi}\frac{\frac{1}{4}\frac{R_S}{\gamma}(g(t')+\gamma^2 T)}{1-\frac{3}{8}\frac{R_S}{\gamma^3}(g(t')+\gamma^2 T)}\,\mathrm{d}t'. \tag{16}$$

(The $\mathrm{d}g/\mathrm{d}t$ term in (15) integrates out.) Equation (16) can be further simplified if $\gamma^3 \gg R_S$ and $\gamma \gg R_S T$. Then

$$\overline{r(t)} \approx -\tfrac{1}{4}R_S T\gamma - \frac{3}{32}\frac{R_S^2}{\gamma^4}\frac{1}{2\pi}\int_0^{2\pi}(g(t')+\gamma^2 T)^2\,\mathrm{d}t'. \tag{17}$$

Since the mean-square amplitude of $g(t)$ has been scaled to $1/\sqrt{2}$

$$\overline{r(t)} \approx -\frac{3}{64}\frac{R_S^2}{\gamma^4} - \tfrac{3}{32}R_S^2 T^2 - \tfrac{1}{4}R_S T\gamma. \tag{18}$$

Equation (18) gives a good indication of the very different behaviour of the fluid system with and without $T = 0$.

3.2. *Trigonometric series technique for sinusoidal forcing*

When $g(t)$ equals $\cos t$ the problem of determining the stability of h can be reduced to finding the roots of a tridiagonal determinant. Following Floquet theory (Stoker 1950), we set

$$u = \sum_{-\infty}^{+\infty} u_n(x)\,\mathrm{e}^{\lambda t}\,\mathrm{e}^{\mathrm{i}nt}, \quad h = \sum_{-\infty}^{+\infty} h_n\,\mathrm{e}^{\lambda t}\,\mathrm{e}^{\mathrm{i}nt}.$$

λ is the Floquet exponent. Substituting the summations into (9) gives

$$\frac{\mathrm{d}^2 u_n}{\mathrm{d}x^2} - (\gamma^2 + 2(\lambda+\mathrm{i}n))\,u_n = \tfrac{1}{2}\gamma(h_{n-1} + 2\gamma^2 T h_n + h_{n+1})\,\mathrm{e}^{-\gamma x}, \tag{19a}$$

$$2(\lambda+\mathrm{i}n)\,h_n = R_S\,u_n, \quad \left.\frac{\mathrm{d}u_n}{\mathrm{d}x}\right|_0 = 0. \tag{19b, c}$$

The solution for u_n is

$$u_n = -\tfrac{1}{2}\gamma(h_{n-1} + 2\gamma^2 T h_n + h_{n+1})\frac{\mathrm{e}^{-\gamma x} - \frac{\gamma}{\zeta_n^{\frac{1}{2}}}\mathrm{e}^{-(\zeta_n)^{\frac{1}{2}}x}}{2(\lambda+\mathrm{i}n)},$$

$$\zeta_n = \gamma^2 + 2(\lambda+\mathrm{i}n).$$

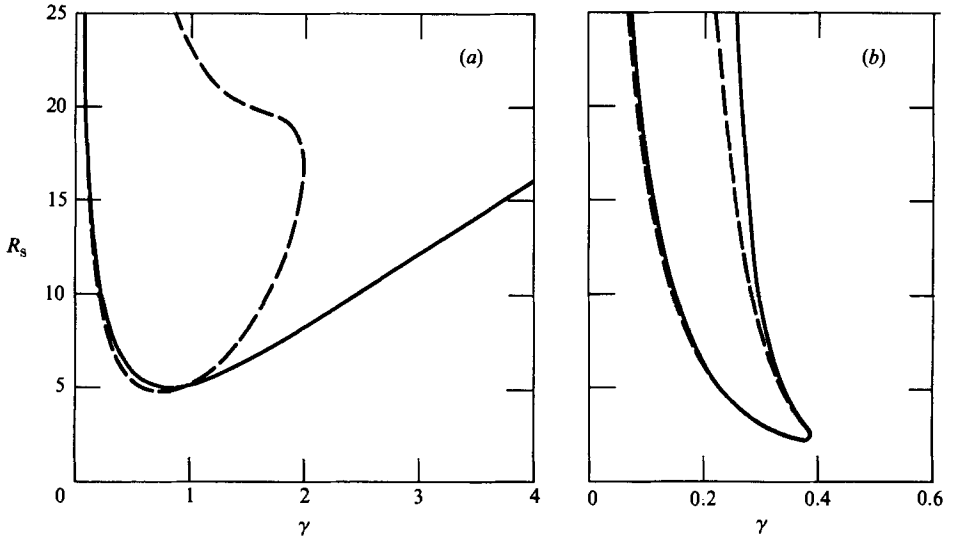

FIGURE 2. The approximate neutral curve (derived from (22)) for the subharmonic-dominated instability for (*a*) $T = 0$, (*b*) $T = 10$. For comparison, the exact curve (dashed) is also shown. Θ_ρ and Θ_μ equal zero.

This can be substituted into (19*b*) to give

$$\left((\lambda+\mathrm{i}n)^2+\tfrac{1}{4}\gamma^3 R_S T\left(1-\frac{\gamma}{\zeta_n^{\frac{1}{2}}}\right)\right)h_n = -\frac{\gamma R_S}{8}\left(1-\frac{\gamma}{\zeta_n^{\frac{1}{2}}}\right)(h_{n-1}+h_{n+1}). \tag{20}$$

A solution of (20) exists only when the infinite tridiagonal determinant formed of the coefficients of the h_n is equal to zero. Approximate roots of this determinant can be found via continued fraction methods, as detailed by Arscott (1964). The searched-for root can be a specific value of any of the parameters λ, R_S, γ, T, ϵ, or δ. Each can thus be found as a function of the other parameters. If root values of R_S, T, ϵ, or δ are sought then standard eigenvalue routines can be applied to truncated versions of (20) as an alternative to the continued fraction approach.

3.3. *Approximate analytical solutions for sinusoidal forcing*

In this section we discuss approximate analytical solutions for (20) for two cases, (i) large γ with $T = 0$ and (ii) small R_S.

We consider first the case of large γ with $T = 0$. By large γ, we mean both that $\gamma \gg 1$ and $\gamma^2 \gg R_S$. Then, as γ increases the equations in (20), except for the equation for h_0, become increasingly diagonally dominant. Concomitantly, the solution for h becomes increasingly dominated by its lowest frequencies. For very large γ, an accurate solution can be found for λ from (20) truncated at $|n| = 1$. The equation determining λ is then

$$\lambda^2 = \frac{\gamma^2 R_S^2}{64}\left(1-\frac{\gamma}{\zeta_0^{\frac{1}{2}}}\right)\frac{1-\left(\dfrac{\gamma}{(\zeta_{-1})^{\frac{1}{2}}}\right)}{(\lambda-\mathrm{i})^2}+\frac{\left(1-\dfrac{\gamma}{(\zeta_{+1})^{\frac{1}{2}}}\right)}{(\lambda+\mathrm{i})^2}. \tag{21}$$

The left and right sides of (21) can balance only when λ is small and when λ is close to $-\gamma^2$. In the first case, $(1-\gamma/\zeta_0^{\frac{1}{2}})$ can be approximated by $\lambda/\gamma^2, (\lambda \pm \mathrm{i})^2$ by -1, and

$(1-\gamma/(\zeta_{\pm 1})^{\frac{1}{2}})$ by $(\pm \mathrm{i}/\gamma^2)+\frac{3}{2}(1/\gamma^4)$ Then, as derived in §3.1, $\lambda \approx -\frac{3}{64}R_S^2/\gamma^4$. In the second case, substitution of $\lambda = -\frac{1}{2}\gamma^2$ into (21) in all terms but $(1-\gamma/\zeta_0^{\frac{1}{2}})$, into which $\lambda = -\frac{1}{2}\gamma^2+\lambda_c$ is substituted, gives

$$\tfrac{1}{4}\gamma^4 \approx \frac{\gamma^2 R_S^2}{32}\frac{\gamma}{\lambda_c^{\frac{1}{2}}}\frac{\gamma}{(-\mathrm{i})^{\frac{1}{2}}}+\frac{\gamma}{\mathrm{i}^{\frac{1}{2}}},$$

from which $\lambda \approx -\frac{1}{2}\gamma^2+\frac{1}{32}R_S^4/\gamma^8$. This quickly decaying mode cannot be found by the asymptotics of §3.1.

The possibility of subharmonic solutions (the imaginary part of λ equaling $\frac{1}{2}$) as $\gamma \to \infty$ can be investigated separately by truncating (20) to the equations for $n = -1$ and $n = 0$. It can be quickly seen, however, that no solutions for large γ are then possible. The same conclusion holds for untuned modes.

We now turn to the case of low Stokes–Reynolds number. For this case the subharmonic dominated mode is the 'most dangerous'. Truncating (20) to $n = -1$ and $n = 0$ and setting the real part of λ to zero, we obtain the following quadratic equation for the subharmonic-dominated-mode neutral curve:

$$(\gamma^6 T^2-\tfrac{1}{4}\gamma^2)\,cc^*R_S^2-\gamma^3 T(c+c^*)\,R_S+1 = 0, \tag{22}$$

where $c = 1-\gamma/(\gamma^2+\mathrm{i})^{\frac{1}{2}}$ and c^* is the complex conjugate of c. For $T = 0$ (22) simplifies to

$$R_S(\lambda = \tfrac{1}{2}\mathrm{i}) = \frac{2}{\gamma}\frac{1}{\left|1-\dfrac{\gamma}{(\gamma^2+\mathrm{i})^{\frac{1}{2}}}\right|}.$$

The approximate neutral curves for $T = 0$ and 10 are shown in figure 2. It can be shown that the maximum unstable wavenumber for $T \gg 1$ is $O(T^{-\frac{2}{3}})$. Equation (22) becomes increasingly accurate as T increases because the relevant γ, and thus the coupling coefficient γR_S in (20), becomes smaller.

A surprising effect of surface tension is that it reduces the critical Stokes–Reynolds number. This reduction is due to the lessening of the importance of viscous damping effects as resonant wavelengths become longer and longer with increasing T. The critical number from (22) is about 4.98 for $T = 0$, 3.28 for $T = 1$, 2.28 for $T = 10$, and 1.95 for $T = 40$. As T increases the neutral curve becomes more and more cusp-like and γ_c, the critical wavenumber, and the γ associated with the double root of (22) become more and more coincident. An approximation to γ_c and the critical Stokes–Reynolds number $(R_S)_c$ can be derived using that fact. We obtain $\gamma_c \approx (2T^2)^{-\frac{1}{6}}$, $(R_S)_c \approx \sqrt{2}+2\gamma_c$. In obtaining these approximations, leading-order inviscid terms cancel out. The approach to the limit is governed by the smaller, viscous-related terms $\gamma/(\gamma^2 \pm \mathrm{i})^{\frac{1}{2}}$ in c and c^*.

3.4. *Numerical results*

Equation (20) was solved using both continued-fraction and eigenvalue methods. For the latter (20) was truncated at $|n| = 24$. The eigenvalue approach was used primarily just to check on some of the continued-fraction results. All numerical results presented here were calculated via the continued-fraction algorithm.

We consider first the case of zero surface tension. Figure 3 shows the computed neutral curves for $T = 0$ in the (γ, R_S)-plane. The lowest banana-shaped curve outlines the subharmonic-dominated instability, the next the harmonic-dominated instability, the next the $\frac{3}{2}$-dominated instability, and so on. Each instability mode is separated from the others by a very thin region of stability. The critical

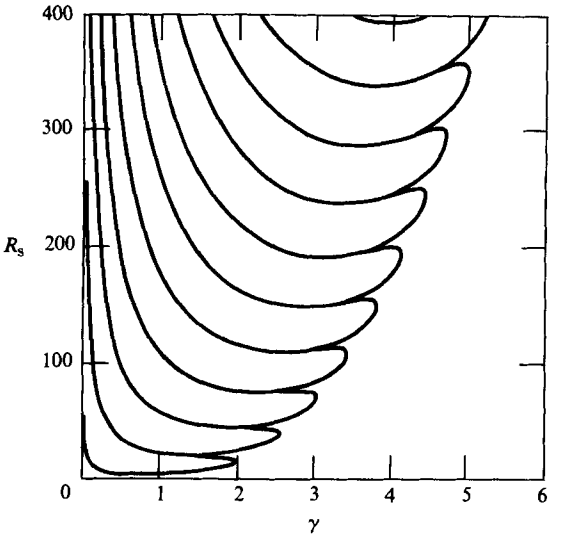

FIGURE 3. Neutral curves in the (γ, R_S)-plane. T, Θ_ρ and Θ_μ equal zero.

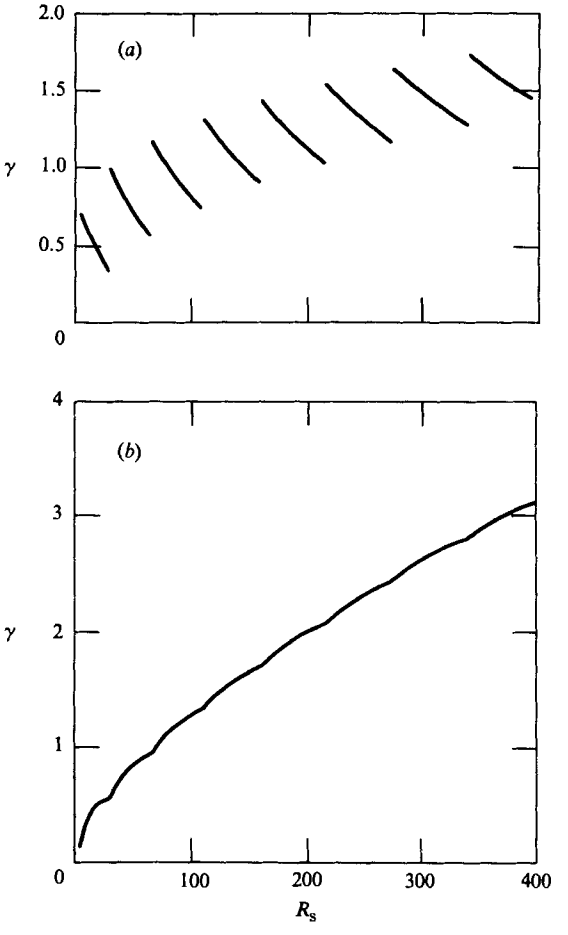

FIGURE 4. Preferred wavenumbers as a function of R_S. (*a*) shows the fastest growing wavenumbers; (*b*) shows their rate of growth (the real part of λ). T, Θ_ρ and Θ_μ equal zero.

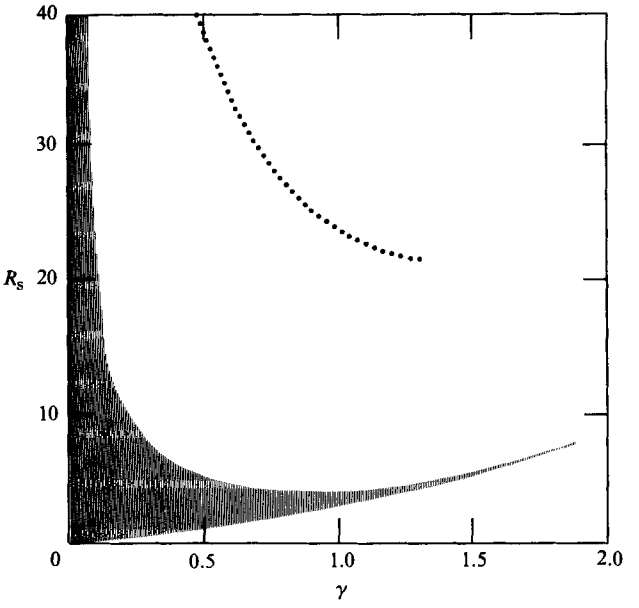

FIGURE 5. The region (shaded) in the (γ, R_S)-plane with untuned eigenmodes. T, Θ_ρ and Θ_μ equal zero.

Stokes–Reynolds number was found to be 4.7681 at a γ of 0.758.The upturnings and high-wavenumber cutoff of the neutral curves in figure 3 are due to viscous effects. The inviscid neutral curves calculable from (10) are hyperbolas that asymptote to both the R_S and γ axes. A quantitative match in position of the viscous and inviscid neutral curves is found in the rather narrow region $\gamma \leqslant 0.05 R_S^{\frac{1}{3}}$.

Figure 4(*a*) graphs the fastest growing wavenumber as a function of R_S. The line breaks whenever there is a shift to a new, higher dominant frequency. For example, the subharmonic-dominated mode is the fastest growing up to $R_S \approx 31$. The harmonic-dominated mode is then the fastest growing up to $R_S \approx 67$. Figure 4(*b*) shows the growth rates of the fastest growing wavenumbers. The increase in preferred dominant frequency and maximum growth rate with R_S is proportional to $R_S^{\frac{2}{3}}$. The preferred wavenumber increases as $R_S^{\frac{1}{3}}$. These dependencies are in agreement with quasi-static results outlined in §3.2.

The general nature of the eigenfunction solutions is also of some interest. First, it was found that, just as for the inviscid case, there are for any given (γ, R_S)-pair only two eigenfunction solutions, of which at most one is unstable. Both eigenfunctions are always of the same type, that is they are both either of subharmonic type, harmonic type, or untuned. The untuned modes are always damped. For the most part these are confined to a region near the $\gamma = 0$ axis, as shown by figure 5. They were also found in some very narrow, virtually one-dimensional, regions that separate the subharmonics from the harmonics. Figure 6 highlights the regions in the (γ, R_S)-plane that have eigenfunctions of harmonic type. Away from the R_S axis, for $R_S \leqslant O(\gamma^3)$, the plane is covered by alternating bands of subharmonic-type and harmonic-type modes.

We now consider the effects of surface tension. Figure 7 shows the most unstable wavenumbers as a function of Stokes–Reynolds number for T equal to 1 and 10. For T equal to 10 the wavelengths of maximum instability are already much longer than for zero surface tension. Also, higher frequency instabilities are inhibited. By

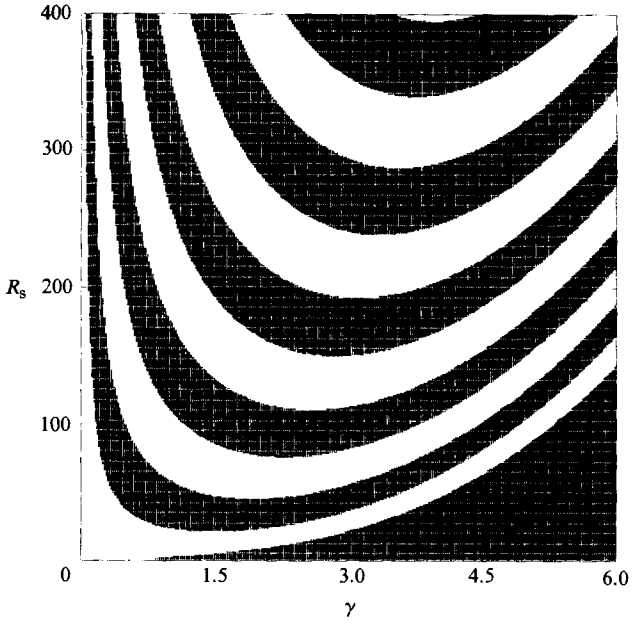

FIGURE 6. Regions (shaded) in the (γ, R_s)-plane that have harmonic-type modes. Except for the corner near $\gamma = 0$ and $R_s = 0$ the unshaded regions have subharmonic-type-mode solutions. T, Θ_ρ and Θ_μ equal zero.

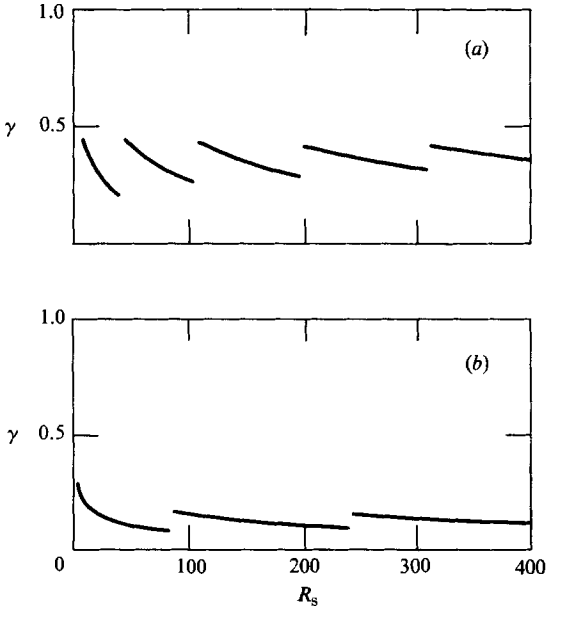

FIGURE 7. Most unstable wavenumbers as a function of R_s for (a) $T = 1$ and (b) $T = 10$. Θ_ρ and Θ_μ equal zero.

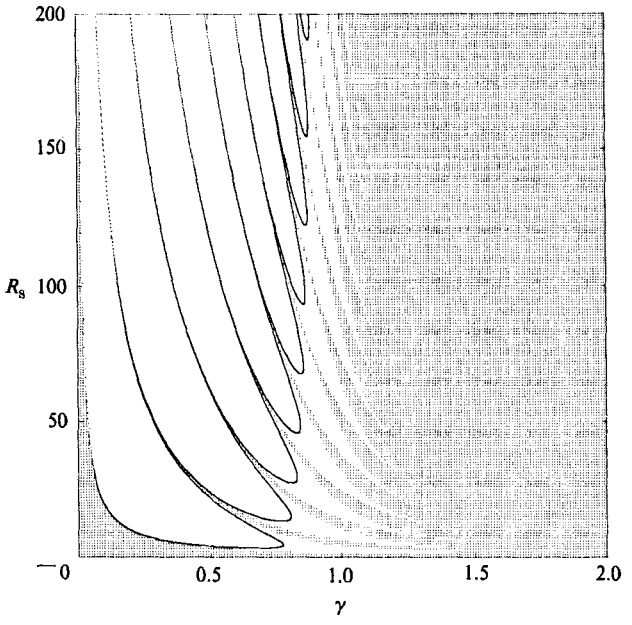

FIGURE 8. Neutral curves and regions of untuned modes (the shaded regions) for $T = 1$. Θ_ρ and Θ_μ equal zero.

$T = 100$ unstable wavenumbers are limited to being less than 0.15. With these longer wavelengths viscous effects are of comparatively little importance. Inviscid and viscous neutral curves are nearly coincident for $T \geqslant 10$ except that the viscous curves exhibit a cusp-like cutoff as discussed in §3.3 while the inviscid instability regions continue (as ever-thinning filaments) as $\gamma \to \infty$. Another effect of even very low surface tension is to make untuned modes predominant in stable regions for all but very large γ. To illustrate this, the neutral curves and the regions of untuned modes for $T = 1$ are shown in figure 8. Perceptibly wide regions of subharmonic- and harmonic-type modes extend only to about γ equal to 1.4. As discussed in §3.1, the harmonic mode becomes important again for very large γ. For example, for $T = 1$ and $R_S = 5$ the transition from untuned modes to the harmonic mode occurs at $\gamma \approx 7.6$.

4. General Θ_ρ and Θ_μ

We now return to the full system of equations (6)–(8). These can be reduced to an infinite tridiagonal matrix in the same fashion as was done in §3.2. The result is

$$\left((\lambda + in)^2 + \tfrac{1}{4}\gamma^3 R_S \frac{b_n}{a_n} T\right) h_n = -\tfrac{1}{8}\gamma R_S \frac{b_n}{a_n}(h_{n-1} + h_{n+1}), \tag{23}$$

with

$$a_n = (\lambda + in)(S_{+,n} + S_{-,n}) + 2\gamma S_{+,n} S_{-,n} + 2\gamma^2 \Theta_\mu (S_{+,n} - S_{-,n}) - 2\gamma^3 \Theta_\mu^2, \tag{24a}$$

$$b_n = (\lambda + in)(S_{+,n} + S_{-,n}); \tag{24b}$$

and with

$$S_{-,n} = \frac{(\lambda + in)(1 - \Theta_\rho)}{(\zeta_{-,n})^{\frac{1}{2}} - \gamma}, \quad S_{+,n} = \frac{(\lambda + in)(1 + \Theta_\rho)}{(\zeta_{+,n})^{\frac{1}{2}} - \gamma}, \tag{25a, b}$$

$$\zeta_{-,n} = \gamma^2 + 2(\lambda + in)\frac{1 - \Theta_\rho}{1 - \Theta_\mu}, \quad \zeta_{+,n} = \gamma^2 + 2(\lambda + in)\frac{1 + \Theta_\rho}{1 + \Theta_\mu}. \tag{25c, d}$$

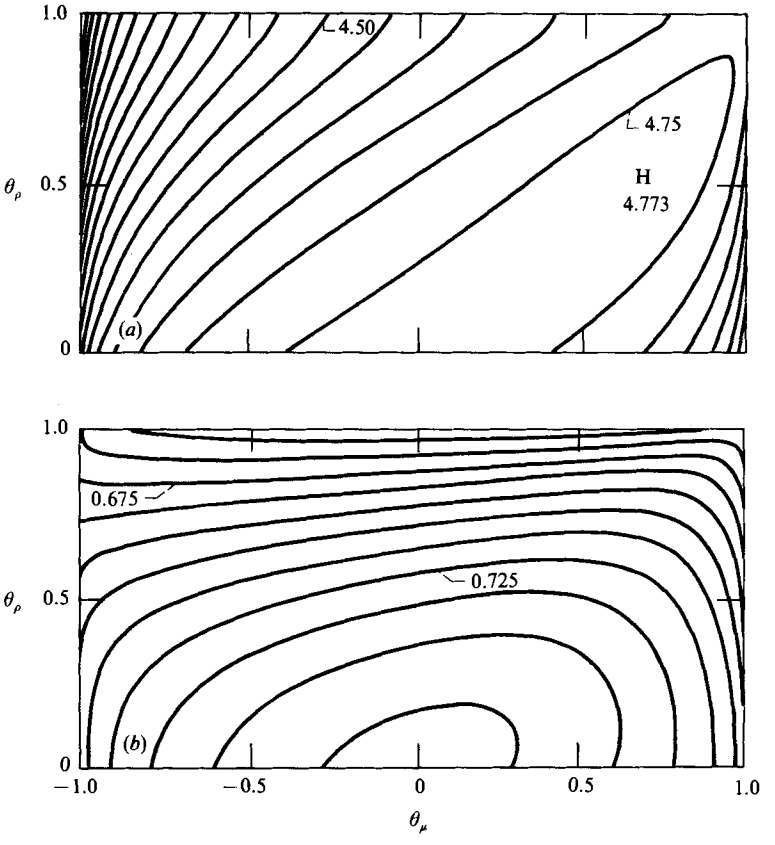

FIGURE 9. (*a*) $(R_S)_c$ and (*b*) γ_c as functions of Θ_ρ and Θ_μ for $T = 0$. Contour intervals for (*a*) are 0.05, for (*b*) 0.01.

Spot checks were made on the sensitivity of the ratio a_n/b_n to variations in Θ_ρ and Θ_μ. In general, it was found to be fairly insensitive. For example, for $n = 1$, $\gamma = 1.24$ and $\lambda = 0$, over the range $-1 \leqslant \Theta_\mu \leqslant 1, 0 \leqslant \Theta_\rho \leqslant 1$, the magnitude of a_n/b_n was found to vary from 1.83 to 2.20 while its phase angle (in rad) ranged from -0.994 to -0.855. For $n = 0$, $\gamma = 0.54$, and $\lambda = 0.5\mathrm{i}$ the magnitude varies from 1.16 to 1.52 and the phase from -0.587 to -0.503. The extent of variation decreases with increasing n and, in general, with increasing γ. Most of the variation of a_n/b_n occurs near $\Theta_\mu = \pm 1$. Its derivative with respect to Θ_μ is singular there.

We have investigated (23) primarily to see how key quantities such as the critical Stokes–Reynolds number and the most unstable wavelengths vary with Θ_ρ and Θ_μ. Figure 9 shows the critical Stokes–Reynolds number and the critical wavenumber as a function of Θ_ρ and Θ_μ for $T = 0$. As could be expected from the moderate sensitivity of a_n/b_n, both critical quantities are fairly insensitive to variations in Θ_ρ and Θ_μ except near $\Theta_\mu = \pm 1$. Figure 10 shows similar results for $T = 10$. The sensitivity of γ_c to Θ_ρ and Θ_μ is reduced substantially as T increases from 0 to 10. as T increases from 0 to 10.

Figure 11 shows the wavenumber and growth rate of the most unstable wave as a function of Θ_ρ and Θ_μ for $R_S = 190$ and $T = 0$. The most unstable mode is of subharmonic type except near $\Theta_\mu = -1$ where a harmonic-type mode with $\gamma \approx 1.35$ is dominant. This jump in mode and corresponding discontinuity in preferred

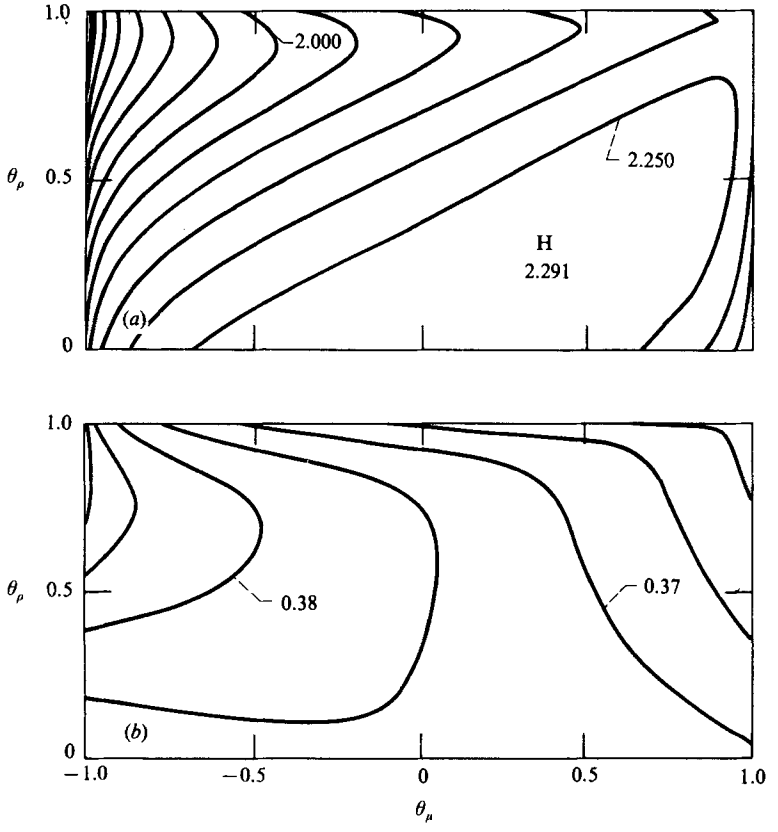

FIGURE 10. (*a*) $(R_S)_c$ and (*b*) γ_c as functions of Θ_ρ and Θ_μ for $T = 10$. Contour intervals for (*a*) are 0.05, for (*b*) 0.005.

wavenumber has already been seen in figure 4(*a*). Except for that discontinuity the preferred wavelength is only weakly sensitive to Θ_ρ and Θ_μ. The growth rate of the most unstable wave is also only weakly sensitive. Preferred wavenumbers and maximum growth rates as a function of Θ_ρ and Θ_μ have been calculated for some Stokes–Reynolds numbers ranging from 20 to 300. All the results show the wavenumber and growth rate having a similar pattern of variation and a similar weak sensitivity to Θ_ρ and Θ_μ.

5. Summary and conclusions

We have shown that oscillating accelerations normal to a fluid density interface with no surface tension can generate very short-wavelength instabilities. With no surface tension, the most unstable wavenumbers and the unstable wavenumber cutoff are both $O(R_S^{\frac{2}{3}})$. Viscous effects are significant for all but very small wavenumbers. They become dominant for $\gamma \gg R_S^{\frac{2}{3}}$ and the fluid system then gives a weakly damped harmonic response to forcing. This is in contrast to the inviscid case in which both the growth rate and frequency of the response increase without bound as $\gamma \to \infty$. Viscosity enforces a critical Stokes–Reynolds number that is a function of Θ_ρ and Θ_μ and has a maximum value of about 4.77.

The fluid system's behaviour changes quite significantly with the introduction of surface tension. In most respects, viscous effects can be neglected for $T \geqslant 10$. An

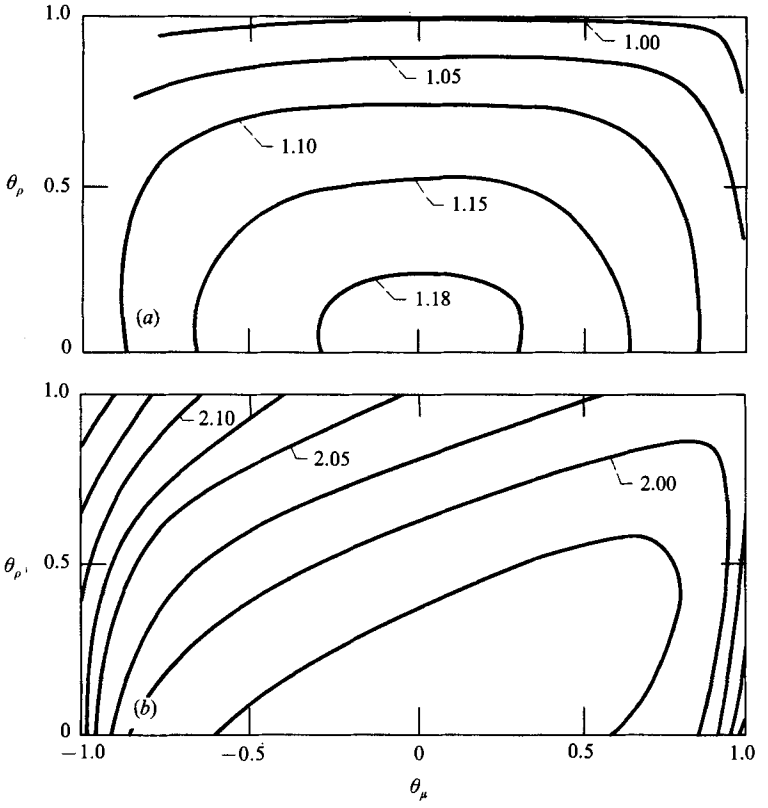

FIGURE 11. (*a*) The most unstable wavenumbers and (*b*) their growth rates for $R_S = 190$ as a function of Θ_ρ and Θ_μ. T equals zero. The most unstable mode is of subharmonic type except at the $\Theta_\mu = -1$ edge of the plot. In (*a*) contours are shown only for the subharmonic-type mode.

important exception is that surface tension and viscosity combine together to limit unstable wavenumbers to $O(T^{-\frac{1}{3}})$. This cutoff actually involves a very slight change in growth rates from the inviscid case, since the inviscid regions of instability above the cutoff are very narrow and only very weakly unstable. Predicted wavelengths for $T \geqslant 10$ are considerably longer than with no surface tension. In practice, container size, neglected in this analysis, may have significant effects on these waves. The critical Stokes–Reynolds number decreases with increasing T, asymptoting to $\sqrt{2}$. This decrease is due to the lessened effect of viscosity as the increasing surface tension excites resonant instabilities at lower and lower wavenumbers.

Our results have indicated that important properties such as the critical Stokes–Reynolds number and the most unstable wavelengths are fairly insensitive to Θ_ρ and Θ_μ. The Boussinesq equal-viscosity approximation discussed in this paper thus appears to be adequate for understanding and predicting most of the instability phenomena of this fluid system.

REFERENCES

ARSCOTT, F. M. 1964 *Periodic Differential Equations*. Macmillan.

BENJAMIN, T. B. & URSELL, F. 1954 The stability of the plane free surface of a liquid in vertical periodic motion. *Proc. R. Soc. Lond.* A **225**, 505.

BURDE, G. I. 1970 Numerical investigation of convection arising in a modulated field of external forces. *Izv. Akad. Nauk SSSR Mzhg* **5**, 196.

CARSLAW, H. S. & JAEGER, J. C. 1959 *Conduction of Heat in Solids* (2nd edn). Oxford University Press.

DODGE, F. T., KANA, D. D. & ABRAMSON, N. 1965 Liquid surface oscillations in longitudinally excited rigid cylindrical containers. *AIAA J.* **3**, 685.

DONNELLY, R. J., REIF, F. & SUHL, H. 1962 Enhancement of hydrodynamic stability by modulation. *Phys. Rev. Let.* **9**, 363.

FARADAY, M. 1831 On a peculiar class of acoustical figures, and on certain forms assumed by groups of particles upon vibrating elastic surfaces. *Phil. Trans. R. Soc. Lond.* **121**, 299.

GALSTER, G. & NIELSEN, F. K. 1984 Crystal growth from solution. In *Proc. 5th European Symposium on Material Sciences under Microgravity.*

GEBHART, B. 1963 Random convection under conditions of weightlessness. *AIAA J.* **1**, 380.

GRESHO, P. M. & SANI, R. L. 1970 The effects of gravity modulation on the stability of a heated fluid layer. *J. Fluid Mech.* **40**, 783.

HASEGAWA, E. 1983 Waves on the interface of two-liquid layers in vertical periodic motion. *JSME Bull.* **26**, 51.

HASEGAWA, E., UMEHARA, T. & ATSUMI, M. 1984 The critical condition for the onset of waves on the free surface of a horizontal liquid layer under a vertical oscillation. *JSME Bull.* **27**, 1625.

HENSTOCK, W. & SANI, R. L. 1974 On the stability of the free surface of a cylindrical layer of fluid in vertical motion. *Lett. Heat Mass Transfer* **1**, 95–102.

KAMOTANI, Y., PRASAD, A. & OSTRACH, S. 1981 Thermal convection in an enclosure due to vibrations aboard spacecraft. *AIAA J.* **19**, 511.

MCLACHLAN, N. W. 1947 *Theory and Application of Mathieu Functions.* Oxford University Press.

MILES, J. W. 1984 Nonlinear Faraday resonance. *J. Fluid Mech.* **75**, 285.

OCKENDON, J. R. & OCKENDON, H. 1973 Resonant surface waves. *J. Fluid Mech.* **59**, 397.

SPRADLEY, L. W., BOURGEOIS, S. V. & LIN, F. N. 1975 Space processing convection evaluation: g-jitter convection of confined fluids in low gravity. *AIAA Paper* 75-695.

STOKER, J. J. 1950 *Nonlinear Vibrations.* Interscience.